Dominant protection from HLA-linked autoimmunity by antigen specific regulatory T cells

Joshua D. Ooi[1*], Jan Petersen[2,3*], Yu H. Tan[2], Megan Huynh[1], Zoe J. Willett[1], Sri H. Ramarathinam[2], Peter J. Eggenhuizen[1], Khai L. Loh[2], Katherine A. Watson[4], Poh-Y. Gan[1], Maliha A. Alikhan[1], Nadine L. Dudek[2], Andreas Handel[5], Billy G. Hudson[6], Lars Fugger[7], David A. Power[8,9], Stephen G. Holt[9,10], P. Toby Coates[11], Jon W. Gregersen[12], Anthony W. Purcell[2], Stephen R. Holdsworth[1,13], Nicole L. La Gruta[2,4], Hugh H. Reid[2,3*], Jamie Rossjohn[2,3,14#] & A. Richard Kitching[1,13,15#]

[1] Centre for Inflammatory Diseases, Monash University Department of Medicine, Monash Medical Centre, Clayton, Victoria 3168, Australia.
[2] Infection and Immunity Program, Biomedicine Discovery Institute and Department of Biochemistry and Molecular Biology, Monash University, Clayton, Victoria 3800, Australia.
[3] Australian Research Council Centre of Excellence in Advanced Molecular Imaging, Monash University, Clayton, Victoria 3800, Australia.
[4] Department of Microbiology and Immunology, The Peter Doherty Institute for Infection and Immunity, The University of Melbourne, Melbourne, Victoria 3000, Australia.
[5] Department of Epidemiology and Biostatistics, College of Public Health, University of Georgia, Athens, GA 30602, USA.
[6] Department of Medicine, Division of Nephrology and Hypertension, Vanderbilt University Medical Center, Nashville, TN 37232, USA.
[7] Oxford Centre for Neuroinflammation, Nuffield Department of Clinical Neurosciences, and MRC Human Immunology Unit, Weatherall Institute of Molecular Medicine, John Radcliffe Hospital, University of Oxford, Oxford OX3 9DS, United Kingdom.
[8] Department of Nephrology, Austin Health, Heidelberg, Victoria 3084, Australia.
[9] Department of Medicine, The University of Melbourne, Melbourne, Victoria 3000, Australia.
[10] Department of Nephrology, The Royal Melbourne Hospital, Parkville, Victoria 3050, Australia.
[11] Central Northern Adelaide Renal and Transplantation Service, Royal Adelaide Hospital, Adelaide, South Australia 5000, Australia.
[12] Department of Medicine, Viborg Regional Hospital, Viborg 8800, Denmark.
[13] Department of Nephrology, Monash Health, Clayton, Victoria 3168, Australia.
[14] Institute of Infection and Immunity, Cardiff University School of Medicine, Heath Park, Cardiff, UK.
[15] Department of Pediatric Nephrology, Monash Health, Victoria, Australia.

* These authors contributed equally to this work

Joint senior and corresponding authors, Hugh.reid@monash.edu, Jamie.rossjohn@monash.edu, Richard.kitching@monash.edu

Susceptibility and protection against human autoimmune diseases, including type I diabetes, multiple sclerosis and Goodpasture's disease, is associated with particular Human Leukocyte Antigen (HLA) alleles. However, the mechanisms underpinning such HLA-mediated effects on self-tolerance remain unclear. Here we investigated the molecular mechanism of Goodpasture's disease, an HLA-linked autoimmune renal disorder characterized by an immunodominant $CD4^+$ T cell self-epitope derived from the α3 chain of Type IV collagen ($\alpha3_{135-145}$)[1-4]. While HLA-DR15 confers a markedly increased disease risk, the protective HLA-DR1 allele is dominantly protective in *trans* with HLA-DR15[2]. We show that autoreactive $\alpha3_{135-145}$-specific T cells expand in patients with Goodpasture's disease and, in $\alpha3_{135-145}$-immunized HLA-DR15 transgenic mice, $\alpha3_{135-145}$-specific T cells infiltrate the kidney and mice develop Goodpasture's disease. HLA-DR15 and HLA-DR1 exhibited distinct peptide repertoires and binding preferences and presented the $\alpha3_{135-145}$ epitope in different binding registers. HLA-DR15-$\alpha3_{135-145}$ $tetramer^+$ T cells in HLA-DR15 transgenic mice exhibit a conventional T cell phenotype (Tconv) that secretes pro-inflammatory cytokines. In contrast, HLA-DR1-$\alpha3_{135-145}$ $tetramer^+$ T cells in HLA-DR1 and HLA-DR15/DR1 transgenic mice are predominantly $CD4^+Foxp3^+$ regulatory T cells (Tregs) expressing tolerogenic cytokines. HLA-DR1-induced Tregs confer resistance to disease in HLA-DR15/DR1 transgenic mice. $HLA\text{-}DR15^+$ and $HLA\text{-}DR1^+$ healthy human donors displayed altered $\alpha3_{135-145}$-specific TCR usage, HLA-DR15-$\alpha3_{135-145}$ $tetramer^+$ $Foxp3^-$ Tconv and HLA-DR1-$\alpha3_{135-145}$ $tetramer^+$ $Foxp3^+CD25^{hi}CD127^{lo}$ Treg dominant phenotypes, and patients with Goodpasture's disease display a clonally expanded $\alpha3_{135-145}$-specific $CD4^+$ T cell repertoire. Accordingly, we provide a mechanistic basis for the dominantly protective effect of HLA in autoimmune disease, whereby HLA polymorphism shapes the relative abundance of self-epitope specific Tregs that leads to protection or causation of autoimmunity.

Using HLA-DR15-$\alpha3_{135-145}$ tetramers, we found that $\alpha3_{135-145}$-specific $CD4^+$ T cells in peripheral blood of $HLA\text{-}DR15^+$ Goodpasture's patients are ~100-fold more frequent than in healthy $HLA\text{-}DR15^+$ donors. Tregs can be important in limiting this disease[5], but in 7 of 8 patients the HLA-DR15-$\alpha3_{135-145}$-specific T cells were mainly $Foxp3^-$ Tconv (**Fig. 1a, Extended Data Table 1**). HLA-DR15-$\alpha3_{135-145}$ $tetramer^+$ $CD4^+$ T cells from all patients recognized $\alpha3_{135-145}$ and α3(IV)NC1 *ex vivo* (**Extended Data Fig. 1a**). After $\alpha3_{135-145}$

immunization, HLA-DR15-$\alpha3_{135\text{-}145}$-specific $CD4^+$ T cells infiltrated diseased kidneys in $DR15^{+.Fcgr2b-/-}$ mice, with the majority of these cells being $Foxp3^-$ (**Fig. 1b, Extended Data Fig. 1b and 1c**). $\alpha3_{135\text{-}145}$ immunized $DR15^{+.Fcgr2b+/+}$ mice, but not HLA-DR1 expressing $DR1^{+.Fcgr2b+/+}$ mice, make pro-inflammatory responses after *ex vivo* stimulation with $\alpha3_{135\text{-}145}$ or α3(IV)NC1, consistent with the lower risk of anti-GBM disease in humans[2]. Furthermore, in $DR15^+DR1^{+.Fcgr2b+/+}$ mice, $\alpha3_{135\text{-}145}$ immunization did not induce pro-inflammatory autoreactivity to $\alpha3_{135\text{-}145}$, or α3(IV)NC1 (**Fig. 1c**). $DR15^+$, $DR1^+$ and $DR15^+DR1^+$ mice had similar overall HLA expression, similar overall proportions of $Foxp3^+$ cells and no TCR Vβ skewing of their entire $CD4^+$ cell repertoire (**Extended Data Fig. 2a**). The dominant negative effect of HLA-DR1 was specific to the area of α3(IV)NC1 containing the immunodominant $\alpha3_{136\text{-}146}$ sequence (**Extended Data Fig. 2b**). Thus, HLA-DR15 restricted pro-inflammatory autoreactivity to $\alpha3_{135\text{-}145}$ is abrogated by co-expression of the HLA-DR1 allele.

Next we characterised the self-peptide repertoires of the HLA-DR15 and HLA-DR1 allomorphs[6-9] from naïve $DR15^+$ and $DR1^+$ mice[10-12]. 5965 HLA-DR15 and 7015 HLA-DR1 bound peptides were identified from which consensus peptide binding motifs were derived using IceLogo[11] (**Fig. 1d**). Coincident with the canonical HLA-DR peptide anchor positions P1, P4, P6/7 and P9, the peptide positions p1, p4, p6 and p9 showed strong but distinct amino acid preferences for HLA-DR15 and HLA-DR1. Findings were similar using human DR15/DR51, and DR1 expressing cell lines (**Extended Data Fig. 3a, 3b and Supplementary Data**).

We hypothesized that the polymorphisms between HLA-DR15 and HLA-DR1 affect the presentation of $\alpha3_{135\text{-}145}$. Here, 9 out of the 13 polymorphic differences reside within the Ag binding cleft (**Fig. 2a**). We solved the structures of HLA-DR15-$\alpha3_{135\text{-}145}$ and HLA-DR1-$\alpha3_{135\text{-}145}$ (**Extended Data Table 2 & Extended Data Fig. 3c-f**). The overall structures of HLA-DR15 and HLA-DR1 were closely matched (0.6 Å r.m.s.d. over 360 Cα-atoms, **Fig. 2a**). In HLA-DR15-$\alpha3_{135\text{-}145}$ the peptide binding register of $\alpha3_{135\text{-}145}$ was GWISLWKGFSF (pHLA positions p1 to p9 underlined), and thus the canonical HLA-DR peptide binding pockets were occupied by the peptide sidechains of p1-Ile, p4-Trp, p7-Phe and p9-Phe (**Fig. 2b**). This peptide binding register was in agreement with the peptide elution data (**Fig. 1d**). Each of the anchor residues (p1-Ile, p4-Trp and p7-Phe) made direct interactions with one or more polymorphic residues of HLA-DR15. Namely, p1-Ile was buried inside the P1 pocket,

where it contacted the polymorphic Val86 (**Figs. 2b and 2e**). p4-Trp lay flat in the P4 pocket and interacted with the polymorphic residues Arg13, Phe26, Asp28 and Ala71. In the adjacent P6/7 pocket, p7-Phe contacted the polymorphic residues Asp28, Tyr30, Phe47 and Ile67. Notably, the P4 and P6/7 pockets were not structurally separated which appeared to be reflected in the enrichment of bulky and aromatic residues in p4 and p7 of HLA-DR15 eluted peptides (**Fig. 1d**).

The peptide binding register of HLA-DR1-$\alpha3_{135\text{-}145}$, GWISLWKGFSF was distinct from HLA-DR15-$\alpha3_{135\text{-}145}$, i.e. it was shifted by one position towards the peptide N-terminus (**Fig 2c**). Interestingly, the binding of $MBP_{85\text{-}99}$ to HLA-DR51 is characterized by a 3 amino acid register shift compared with its binding to HLA-DR15[13]. Overlay of the peptides bound by HLA-DR15 and HLA-DR1 showed a difference in the peptide backbone conformations largely attributable to a flipped peptide bond between p5 and p6, resulting in differences of p6, p7 and p8 Cα-positions of 2.2 Å, 2.5 Å and 1.5 Å, respectively (**Fig. 2d**). The peptide in HLA-DR1-$\alpha3_{135\text{-}145}$ was anchored via the residues p1, p4, p6 and p9. The register shift was accompanied with a positional switch of the peptide anchor residue residing in the P6/P7 pocket (p6-Lys in HLA-DR1 and p7-Phe in HLA-DR15). The observed peptide binding register shift was in agreement with the peptide elution data of HLA-DR1 (**Fig. 1d)**, as it placed the preferred anchor residues p1-Trp and p4-Leu in the P1 and P4 pockets, respectively (**Figs. 2c and 2f**). Compared to P1 of HLA-DR15, the P1 pocket of HLA-DR1 had a 190 $Å^3$ larger volume due to the polymorphic residue Gly86 (Val86 in HLA-DR15). This allowed P1 of HLA-DR1 to accommodate p1-Trp, whilst P1 of HLA-DR15 would be unable to accommodate a Trp residue. The P4 and P6/7 pockets of HLA-DR1 were structurally segregated by the polymorphic residue Arg71 (Ala71 in HLA-DR15). This restricted the available space in the P4 pocket when compared to HLA-DR15. Compared to HLA-DR15, P6/7 of HLA-DR1 provided additional space underneath the peptide due to the presence of Cys30 and Phe13 (Tyr30 and Arg13 in HLA-DR15). Therefore, differences in shape and aperture of the P6/7 pocket allowed p6-Lys to reach underneath the peptide and act as a peptide anchor residue in HLA-DR1 forming a salt bridge with Glu28 (**Fig. 2f**), whereas HLA-DR15 p7-Phe bound laterally with respect to the peptide. Thus, the dominant negative effect of HLA-DR1 in anti-GBM disease is accompanied by register-shifted binding of $\alpha3_{135\text{-}145}$ to HLA-DR1 and consequently a distinctly different peptide-HLA landscape.

We next addressed whether this altered pHLA landscape caused differences in the responding T cell repertoire (**Fig. 2g**). Namely, HLA-DR1-$\alpha3_{135\text{-}145}$ restricted T cells from $DR1^+$ mice were more likely to bear TRAV14 than HLA-DR15-$\alpha3_{135\text{-}145}{}^+$ T cells from $DR15^+$ mice. In contrast, HLA-DR15-$\alpha3_{135\text{-}145}$ restricted TCRs exhibited TRBV bias, with TRBV19 present in 17/100 T cells, but absent in the HLA-DR1-$\alpha3_{135\text{-}145}$ T cell repertoire. Notably, experiments in $DR15^+DR1^+$ mice showing DR1-$\alpha3_{135\text{-}145}$ TRAV14 usage and DR15-$\alpha3_{135\text{-}145}$ TRBV19 usage demonstrated that even in the presence of both HLA-DR15 and HLA-DR1, $\alpha3_{135\text{-}145}$-specific TCR usage is determined by the individual HLA molecule in a similar manner to mice transgenic for either HLA-DR15 or HLA-DR1 (**Fig. 2g**). We also found significant differences in the overall TCR distribution in the TRAJ region usage in the $\alpha3_{135\text{-}145}$ TCR repertoire between $DR15^+$ and $DR1^+$ mice (**Extended Data Fig. 4a**). These findings demonstrate that the altered pHLA landscapes result in differences in the responding T cell repertoire

Next, we ascertained whether differences in $\alpha3_{135\text{-}145}$-specific TCR usage between HLA-DR15 and HLA-DR1 were accompanied by functional phenotypic differences. We found that $CD4^+$ T cells specific for this epitope from naive $DR15^+$ mice were largely $CD4^+Foxp3^-$ conventional T cells (Tconvs). In contrast, in $DR1^+$ mice, $\alpha3_{135\text{-}145}$-specific $CD4^+Foxp3^+$ Tregs were predominant, with their gene expression pattern being consistent with thymically derived tTregs (**Extended Data Fig. 4b**). In $DR15^+DR1^+$ mice, HLA-DR15-$\alpha3_{135\text{-}145}$ $tetramer^+$ $CD4^+$ cells were largely $Foxp3^-$ Tconvs and those that bound the HLA-DR1-$\alpha3_{135\text{-}145}$ tetramer were largely $Foxp3^+$ Tregs (**Fig. 3a**). Culture of naive $CD4^+$ cells and syngeneic APCs with or without $\alpha3_{135\text{-}145}$ peptide showed that $\alpha3_{135\text{-}145}$-specific cells from $DR15^+$ mice produced interferon-γ (IFN-γ), interleukin-17A (IL-17A) and IL-6, whereas those from $DR1^+$ and $DR15^+DR1^+$ mice did not produce these pathogenic T helper cell 1 (Th1) and Th17 cytokines (**Fig. 3b**)[4,14]. When $CD4^+CD25^+$ Tregs were removed prior to culture, pro-inflammatory $\alpha3_{135\text{-}145}$-specific responses emerged in $DR15^+DR1^+$ mice, but not in $DR1^+$ mice (**Fig. 3b**) indicating that in cultures from $DR15^+DR1^+$ mice, Tregs prevent the development of $\alpha3_{135\text{-}145}$-specific pro-inflammatory responses. When Tregs were present in $DR1^+$ and in $DR15^+DR1^+$ mice, $Foxp3^+$ Tregs proliferated in an antigen specific manner and secreted IL-10 and transforming growth factor-β (TGF-β) in response to $\alpha3_{135\text{-}145}$ peptide (**Fig. 3b, Extended Data Fig. 5a**). Furthermore, Tregs from $DR1^+$ mice were substantially

more potent in suppressing the development of $\alpha3_{136-146}$-induced responses in $CD4^+CD25^-$ T cells from $DR15^+DR1^+$ mice when they included $\alpha3_{135-145}$-specific Tregs (**Extended Data Fig. 5b**). Therefore, HLA-DR1's dominant protection from the HLA-DR15 conferred risk of anti-GBM disease is via the induction of $\alpha3_{135-145}$-specific Tregs.

We assessed the capacity of Tregs *in vivo* to prevent autoimmunity to $\alpha3_{135-145}$ using HLA transgenic mice in experimental Goodpasture's disease. Consistent with the *in vitro* findings (**Fig. 3b**), HLA-$DR15^+$ mice developed reactivity towards $\alpha3_{135-145}$, with or without Treg depletion, while even after Treg depletion $DR1^+$ mice did not develop pro-inflammatory reactivity to $\alpha3_{135-145}$ after immunization with this peptide. However, in $DR15^+DR1^+$ mice, Treg depletion unmasked significant autoreactivity, with evidence of Th1 and Th17 responses (**Fig. 3c**)[4,14]. Furthermore, Treg depletion in $DR15^+DR1^+$ mice resulted in an expanded population of HLA-DR15-$\alpha3_{135-145}$ $tetramer^+$ T follicular helper (Tfh) cells after immunization (**Extended Data Fig. 5c**), which would permit the induction of the classical anti-GBM (anti-α3(IV)NC1) autoantibodies found in this disease. To determine if Treg depletion unmasks Goodpasture's disease itself in the presence of both HLA-DR15 and HLA-DR1, we immunized $DR15^{+.Fcgr2b-/-}$, $DR1^{+.Fcgr2b-/-}$ and $DR15^+DR1^{+.Fcgr2b-/-}$ mice with $\alpha3_{135-145}$ peptide, with or without Treg depletion (**Fig. 4a,**). In Treg depleted mice, $CD4^+Foxp3^+$ Tregs were reduced at days 7 and 14 during the development of autoimmunity, but restored by day 21 (**Extended Data Fig. 6a**) and mice immunized with a control peptide ($OVA_{323-339}$) did not develop disease (**Extended Data Fig. 6b**). $DR15^{+.Fcgr2b-/-}$ mice developed anti-GBM disease (**Fig. 4a, Extended Data Fig. 6c and 6d**), with no significant increase in most parameters after early Treg depletion. $DR1^{+.Fcgr2b-/-}$ mice were protected from disease after $\alpha3_{135-145}$ immunization and Treg depletion did not provoke renal disease. $DR15^+DR1^{+.Fcgr2b-/-}$ mice did not develop disease, demonstrating the dominant protection of HLA-DR1 *in vivo* in this system. Critically, after Treg depletion $\alpha3_{135-145}$ immunized $DR15^+DR1^{+.Fcgr2b-/-}$ mice developed severe glomerulonephritis of similar severity to $DR15^{+.Fcgr2b-/-}$ mice, phenotypically similar to human anti-GBM disease, with the classical and diagnostic serum anti-α3(IV)NC1 autoantibodies and IgG deposition on the GBM as well as glomerular infiltration of effector cells and elevated mRNA for intrarenal pro-inflammatory cytokines (**Fig. 4a, Extended Data Fig. 6c and 6d**). Therefore, endogenous HLA-DR1-associated $\alpha3_{135-145}$-specific Tregs abrogate the DR15 mediated increased risk of developing Goodpasture's disease and dominantly protect from this autoimmune disease.

Next we examined $\alpha3_{135\text{-}145}$-specific $CD4^+$ T cells from fully HLA-typed healthy blood donors who were either HLA-DR15 homozygotes, HLA-DR1 homozygotes or DR15/DR1 heterozygotes (**Extended Data Table 3**). The HLA-DR15-$\alpha3_{135\text{-}145}$-specific $CD4^+$ T cells from donors homozygous for HLA-DR15 were largely $Foxp3^-$ Tconvs, those in people homozygous for DR1 were $Foxp3^+CD25^{hi}CD127^{lo}$ Tregs, while in DR15/DR1 heterozygotes, the HLA-DR15-$\alpha3_{135\text{-}145}$ $tetramer^+$ $CD4^+$ T cells were Tconvs and HLA-DR1-$\alpha3_{135\text{-}145}$ $tetramer^+$ $CD4^+$ T cells were Tregs (**Fig. 4b**). Only $CD4^+$ cells from healthy HLA-DR15 homozygote donors secreted pro-inflammatory cytokines in response to $\alpha3_{135\text{-}145}$ in the presence of Tregs. When $CD25^{hi}CD127^{lo}$ cells were removed prior to culture, pro-inflammatory responses emerged in T cells from DR15/DR1 heterozygotes, but not HLA-DR1 homozygote healthy donors, while in the context of DR1 Tregs exhibited $\alpha3_{135\text{-}145}$-specific proliferation and cytokine production (**Fig. 4c**). The $\alpha3_{135\text{-}145}$-specific $CD4^+$ T cell repertoire also showed evidence of skewing, in the TRBV gene usage (**Extended Data Fig. 7a**). We also examined the $\alpha3_{135\text{-}145}$-specific TCR repertoire in the peripheral blood of two Goodpasture's patients with acute disease and found that conserved HLA-DR15-$\alpha3_{135\text{-}145}$-specific $CD4^+$ TCR sequences were present in both the TRAV and TRBV regions (**Extended Data Fig. 7b**) of both patients, particularly in patient GP1 who exhibited identical sequences in 6/12 TRAV and 4/16 TRBV analyses. The repeat sequences in HLA-DR15-$\alpha3_{135\text{-}145}$ $tetramer^+$ $CD4^+$ T cells in patients with Goodpasture's disease provide further evidence that the $\alpha3_{135\text{-}145}$ epitope plays a pivotal role in this disease.

Other autoimmune diseases with HLA associations, including type I diabetes and multiple sclerosis have reported dominantly protective or modulatory HLA alleles[15-17]. Presently, the mechanisms underpinning such dominant protective HLA effects are unclear, although several theories, including epitope capture, T cell deletion and Treg dominance have been proposed. Here, we have used Goodpasture's disease as a model human autoimmune disease to mechanistically determine how an HLA allele can exert its dominant protective effect. Our structural and T cell repertoire data show that neither epitope capture nor T cell deletion are the mechanisms at play here. Instead, the dominant protective effect of HLA-DR1 is associated with $\alpha3_{135\text{-}145}$-specific Tregs. In Goodpasture's disease, a register shift in the binding of the immunodominant autoreactive peptide to HLA-DR1 compared to HLA-DR15 leads to fundamental differences between their $CD4^+$ $\alpha3_{135\text{-}145}$-specific TCR repertoire and

phenotype. Our studies therefore provide a mechanistic basis for understanding HLA-mediated susceptibility and protection in autoimmune disease.

REFERENCES

1 Hudson, B. G., Tryggvason, K., Sundaramoorthy, M. & Neilson, E. G. Alport's syndrome, Goodpasture's syndrome, and type IV collagen. *N Engl J Med* **348**, 2543-2556 (2003).

2 Phelps, R. G. & Rees, A. J. The HLA complex in Goodpasture's disease: a model for analyzing susceptibility to autoimmunity. *Kidney Int* **56**, 1638-1653 (1999).

3 Cairns, L. S. *et al.* The fine specificity and cytokine profile of T-helper cells responsive to the alpha3 chain of type IV collagen in Goodpasture's disease. *J Am Soc Nephrol* **14**, 2801-2812 (2003).

4 Ooi, J. D. *et al.* The HLA-DRB1*15:01-Restricted Goodpasture's T Cell Epitope Induces GN. *J Am Soc Nephrol* **24**, 419-431 (2013).

5 Salama, A. D. *et al.* Regulation by CD25+ lymphocytes of autoantigen-specific T-cell responses in Goodpasture's (anti-GBM) disease. *Kidney Int* **64**, 1685-1694 (2003).

6 Hammer, J., Takacs, B. & Sinigaglia, F. Identification of a motif for HLA-DR1 binding peptides using M13 display libraries. *J Exp Med* **176**, 1007-1013 (1992).

7 Vogt, A. B. *et al.* Ligand motifs of HLA-DRB5*0101 and DRB1*1501 molecules delineated from self-peptides. *J Immunol* **153**, 1665-1673 (1994).

8 Mohme, M. *et al.* HLA-DR15-derived self-peptides are involved in increased autologous T cell proliferation in multiple sclerosis. *Brain* **136**, 1783-1798 (2013).

9 Clement, C. C. *et al.* The Dendritic Cell Major Histocompatibility Complex II (MHC II) Peptidome Derives from a Variety of Processing Pathways and Includes Peptides with a Broad Spectrum of HLA-DM Sensitivity. *J Biol Chem* **291**, 5576-5595 (2016).

10 Dudek, N. L., Croft, N. P., Schittenhelm, R. B., Ramarathinam, S. H. & Purcell, A. W. A Systems Approach to Understand Antigen Presentation and the Immune Response. *Methods Mol Biol* **1394**, 189-209 (2016).

11 Scally, S. W. *et al.* A molecular basis for the association of the HLA-DRB1 locus, citrullination, and rheumatoid arthritis. *J Exp Med* **210**, 2569-2582 (2013).

12 Illing, P. T. *et al.* Immune self-reactivity triggered by drug-modified HLA-peptide repertoire. *Nature* **486**, 554-558 (2012).

13 Li, Y., Li, H., Martin, R. & Mariuzza, R. A. Structural basis for the binding of an immunodominant peptide from myelin basic protein in different registers by two HLA-DR2 proteins. *J Mol Biol* **304**, 177-188 (2000).
14 Ooi, J. D., Phoon, R. K., Holdsworth, S. R. & Kitching, A. R. IL-23, not IL-12, directs autoimmunity to the Goodpasture antigen. *J Am Soc Nephrol* **20**, 980-989 (2009).
15 Todd, J. A. & Wicker, L. S. Genetic protection from the inflammatory disease type 1 diabetes in humans and animal models. *Immunity* **15**, 387-395 (2001).
16 Gregersen, J. W. *et al.* Functional epistasis on a common MHC haplotype associated with multiple sclerosis. *Nature* **443**, 574-577 (2006).
17 van der Horst-Bruinsma, I. E. *et al.* HLA-DQ-associated predisposition to and dominant HLA-DR-associated protection against rheumatoid arthritis. *Hum Immunol* **60**, 152-158 (1999).

Supplementary Information is available in the online versions of the paper.

Acknowledgements We thank the staff of the Australian Synchrotron (beamline MX1) for assistance with data collection and donors of the Australian Bone Marrow Donor Registry for blood samples. This study was supported by grants from the National Health and Medical Research Council of Australia (NHMRC), 1048575 to A.R.K., 334067 to A.R.K. and S.R.H., A.W.P. is supported by an NH&MRC Senior Research Fellowship, J.R. is supported by an Australian Research Council Laureate Fellowship.

Author contributions J.D.O., J.P., H.H.R, J.R. and A.R.K. initiated and designed the research and wrote the manuscript. J.D.O., J.P., Y.H.T., M.H., Z.J.W., N.L.D., P.J.E., K.L.L, K.A.W., P.Y.G., M.A.A, and S.H.R. performed experiments. D.A.P., S.G.H., P.T.C., J.W.G. provided Goodpasture's patients' blood samples and clinicopathological information. A.H., B.G.H., L.F., A.W.P., S.R.H., N.L.L.G. provided intellectual input and technical support. J.D.O. and J.P. are equal first authors. H.H.R., J.R. and A.R.K. are the co-senior and co-corresponding authors.

Author Information Reprints and permissions information is available at www.nature.com/reprints. The authors declare no competing interests. Readers are welcome to comment on the online version of the paper. Correspondence and requests for materials

should be addressed to H.H.R. (hugh.reid@monash.edu), J.R. (jamie.rossjohn@monash.edu) or A.R.K. (richard.kitching@monash.edu).

FIGURE LEGENDS

Figure 1: $\alpha3_{135\text{-}145}$ induces nephritogenic autoimmunity, but not when DR1 is co-expressed. a, $\alpha3_{135\text{-}145}$-specific Foxp3$^-$ effector CD4$^+$ T cells in DR15$^+$ healthy humans (n=7), and Goodpasture's (GP) patients (n=8). **b**, $\alpha3_{135\text{-}145}$-specific effector CD4$^+$ T cells in kidneys from $\alpha3_{135\text{-}145}$-immunized DR15$^{+.Fcgr2b-/-}$ mice (n=5 each group). **c**, HLA-DR1 co-expression prevents pro-inflammatory autoreactivity to the GP antigen in $\alpha3_{135\text{-}145}$-immunized DR15$^+$DR1$^{+.Fcgr2b+/+}$ mice (n=4 each group). **d**, Peptide repertoire analyses of HLA-DR presented self-peptides in DR15$^+$ and DR1$^+$ transgenic mice. Enriched and depleted amino acids are above and below the horizontal bar, respectively, scale of letter proportional to frequency difference. Values are mean±s.e.m.; $^*P$<0.05; $^{**}P$<0.01; $^{***}P$<0.001 by Mann-Whitney U test (**a**, **b**) or Kruskal-Wallis test (**c**).

Figure 2: Presentation of $\alpha3_{135\text{-}145}$ by HLA-DR15 and HLA-DR1. a, Polymorphisms (red) with the β-chains of HLA-DR15 (light blue) and HLA-DR1 (light yellow). **b-f**, HLA-DR15-$\alpha3_{135\text{-}145}$ and HLA-DR1-$\alpha3_{135\text{-}145}$ with HLA-DR α-chain (light green). Black, red and brown dashes represent H-bonds, salt-bridges, and peptide pocket positions, respectively. **b**, HLA-DR15-$\alpha3_{135\text{-}145}$ **c,** HLA-DR-$\alpha3_{135\text{-}145}$. **d**, HLA-DR15 and HLA-DR1 alignment. **e**, HLA-DR15 and DR1 polymorphisms (**f**) and interactions with $\alpha3_{135\text{-}145}$. **g**, TRAV and TRVB chain usage of $\alpha3_{135\text{-}145}$-specific CD4$^+$ T cells in HLA-DR transgenic mice (pooled samples, n=3 mice each group), and phenotyping for Vα2 (TRAV14) and Vβ6 (TRBV19). Frequencies of TCRs between DR15 and DR1 were compared by Fisher's exact test *** P<0.001. For flow cytometry, n=4 individual mice per group, $^*P$<0.05, *** P<0.001 by unpaired two-tailed t-test.

Figure 3: DR15 selects $\alpha3_{135\text{-}145}$-specific Tconvs but DR1 selects protective Tregs. a, $\alpha3_{135\text{-}145}$-specific CD4$^+$ T cells from naïve HLA-DR transgenic mice are predominantly Tconv (Foxp3$^-$) in the context of HLA-DR15, but Tregs (Foxp3$^+$) are selected by HLA-DR1. **b**, Naive CD4$^+$ T cells from DR15$^+$ mice with intact Tregs stimulated by $\alpha3_{135\text{-}145}$ secrete pro-inflammatory cytokines, cells from DR1$^+$ and DR15$^+$DR1$^+$ mice secrete tolerogenic cytokines, but without Tregs, T cells from DR15$^+$ mice become autoreactive. Only in cells

from mice bearing HLA-DR1 does $\alpha3_{135\text{-}145}$ induce Treg proliferation. Cells were pooled from three mice of each strain, representative of three independent experiments performed in triplicate. **c**, *In vivo* depletion of Tregs results in autoreactivity in immunized $DR15^{+}DR1^{+.Fcgr2b+/+}$ mice (n=4 each group). Values are mean±s.e.m.; $^{*}P<0.05$, $^{**}P<0.01$, $^{***}P<0.001$ by Mann Whitney U test.

Figure 4: Treg depletion unmasks disease in $DR15^{+}DR1^{+.Fcgr2b-/-}$ mice and autoimmunity in humans *in vitro*. **a**, Treg depletion before $\alpha3_{135\text{-}145}$ immunization leads to anti-GBM glomerulonephritis in $DR15^{+}DR1^{+.Fcgr2b-/-}$ mice ($DR15^{+.Fcgr2b-/-}$ n=6 each group, $DR1^{+}$ $^{Fcgr2b-/-}$ n=4 each group and $DR15^{+}DR1^{+.Fcgr2b-/-}$ n=8 [Treg intact], 9 [Treg depleted]). Scale bars = 30 μm. **b**, In the blood of healthy HLA-typed humans, $\alpha3_{135\text{-}145}$-specific $CD4^{+}$ Tconv cells predominate in the setting of DR15 and Tregs with DR1. **c**, In humans, only $CD4^{+}$ T cells from healthy DR15 homozygotes (n=6) exhibit pro-inflammatory autoreactivity to $\alpha3_{135\text{-}145}$ when Tregs are present, while Tregs in DR1 homozygotes (n=5) and DR15/DR1 heterozygotes (n=5) proliferate and secrete tolerogenic cytokines. Values are mean±s.e.m.; $^{*}P<0.05$; $^{**}P<0.01$; $^{***}P<0.001$**,** by unpaired two-tailed t-test (**a, c** top panels), Mann Whitney U test (**b**) and Kruskal-Wallis test **(c**, bottom panel).

METHODS

Human subjects. Patients who were included in the study all had Goodpasture's disease and fulfilled the key diagnostic criteria: 1) serum anti-α3(IV)NC1 IgG by ELISA, 2) linear IgG staining of the GBM and 3) necrotizing and crescentic glomerulonephritis. HLA-DR15 typing of patients was done by monoclonal antibody staining (BIH0596, One Lambda) and flow cytometry. Blood from HLA-typed healthy humans was collected via the Australian Bone Marrow Donor Registry (ABMDR). HLA-DR15, HLA-DR1 and HLA-DR15/DR1 donors were molecularly typed and were excluded if they expressed DQB1*03:02, which is potentially weakly associated with susceptibility to anti-GBM disease[2]. Studies were approved by the ABMDR and Monash Health Research Ethics Committees, and informed consent was obtained from each individual.

Humanised HLA transgenic mice. Mouse MHCII deficient, DR15 transgenic mice and mouse MHCII deficient, DR1 transgenic mice were derived from existing HLA transgenic colonies and intercrossed so that they are on the same background as previously described[4]. Background: 50% C57BL/10, 43.8% C57BL/6, 6.2% DBA/2; or with an *Fcgr2b*$^{-/-}$ background: 72% C57BL/6, 25% C57BL/10 and 3% DBA/2. To generate mice transgenic for both HLA-DR15 and HLA-DR1 mice transgenic for either HLA-DR15 or HLA-DR1 were intercrossed. FcγRIIb intact HLA transgenic mice and cells were used for all experiments, except experiments in experimental Goodpasture's disease, where *Fcgr2b*$^{-/-}$ HLA transgenic strains were used. While DR15^{+} mice readily break tolerance to α3(IV)NC1 when immunized with human $\alpha3_{135\text{-}145}$ or mouse $\alpha3_{136\text{-}146}$, renal disease is mild[4]. As genetic changes in Fc receptors have been implicated in the development of nephritis in rodents and in humans[18], *Fcgr2b*$^{-/-}$ HLA transgenic strains were used when end organ injury was an important endpoint. Experiments were approved by the Monash University Animal Ethics Committee (MMCB2011/05 and MMCB2013/21).

Expression and purification of recombinant HLA-DR molecules. HLA-DR15-$\alpha3_{135\text{-}145}$ and HLA-DR1-$\alpha3_{135\text{-}145}$ were produced in High Five insect cells (*Trichoplusia ni* BTI-TN-5B1-4 cells, Invitrogen) using the baculovirus expression system essentially as described previously for HLA-DQ2/DQ8 proteins[19,20]. Briefly, synthetic DNA (Integrated DNA Technologies, IA) encoding the α- and β-chain extracellular domains of HLA-DR15 (HLA-DR1A*0101, HLA-DRB1*15:01) HLA-DR1 (HLA-DR1A*0101, HLA-DRB1*01:01), and

the $\alpha3_{135\text{-}145}$ peptide were cloned into the pZIP3 baculovirus vector[19,20]. To promote correct pairing, the C-termini of the HLA-DR15 and HLA-DR1 α- and β-chain encode enterokinase cleavable Fos and Jun leucine zippers, respectively. The β-chains also encoded a C-terminal BirA ligase recognition sequence for biotinylation and a poly-histidine tag for purification. HLA-DR15-$\alpha3_{135\text{-}145}$ and HLA-DR1-$\alpha3_{135\text{-}145}$ were purified from baculovirus infected High Five insect cell supernatants via successive steps of immobilized metal ion affinity (Ni Sepharose 6 Fast-Flow, GE Healthcare), size exclusion (S200 Superdex 16/600, GE Healthcare) and anion-exchange (HiTrap Q HP, GE Healthcare) chromatography. For crystallization, the leucine zipper and associated tags were removed by enterokinase digestion (Genscript, NJ) further purified by anion exchange chromatography, buffer exchanged into 10 mM Tris, pH 8.0, 150 mM NaCl and concentrated to 7 mg/ml.

Tetramer generation and sample analysis. Purified HLA-DR15-$\alpha3_{135\text{-}145}$ and HLA-DR1-$\alpha3_{135\text{-}145}$ proteins were buffer exchanged into 10 mM Tris pH 8.0, biotinylated using BirA ligase and tetramers assembled by addition of Streptavidin-PE (BD Biosciences) as previously described[19]. In mice, 10^7 splenocytes or cells from kidneys digested with 5 mg/ml collagenase D (Roche Diagnostics, Indianapolis, IN) and 100 mg/ml DNase I (Roche Diagnostics) in HBBS (Sigma-Aldrich) for 30 minutes at 37°C, filtered, erythrocytes lysed, and the $CD45^+$ leukocyte population isolated by MACS using mouse CD45 microbeads (Miltenyi Biotec), were surface stained with Pacific Blue labeled anti-mouse CD4 (BD), APC-Cy7 labeled anti-mouse CD8 (BioLegend) and 10 nM of PE-labeled tetramer. Cells were then incubated with a Live/Dead fixable Near IR Dead Cell Stain (Thermo Scientific), permeabilized using a Foxp3 Fix/Perm Buffer Set (BioLegend), and stained with Alexa Fluor 647 labeled anti-mouse foxp3 antibody (FJK16s). To determine Vα2 and Vβ6 usage, cells were stained with PerCP/Cy5.5 anti-mouse Vα2 (B20.1, Biolegend) and APC labelled anti-mouse Vβ6 (RR4-7, Biolegend). For each mouse a minimum of 100 cells were analysed. The $tetramer^+$ gate was set based on the $CD8^+$ population. In humans, $3x10^7$ white blood cells were surface stained with BV510 labeled anti-human CD3 (BioLegend), Pacific Blue labeled anti-human CD4 (BioLegend), PE-Cy7 labelled anti-human CD127 (BioLegend), FITC labelled anti-human CD25 (BioLegend) and 10 nM of PE-labeled tetramer. Then, cells were incubated with a Live/Dead fixable Near IR Dead Cell Stain (Life Technologies), permeabilized using a Foxp3 Fix/Perm Buffer Set (BioLegend), and stained with Alexa Fluor 647 labeled anti-human Foxp3 antibody (150D). The tetramer positive gate was set based on

the $CD3^+CD4^-$ population. As validation controls, we found that HLA-DR1-$\alpha3_{135-145}$ $tetramer^+$ cells did not bind to HLA-DR1-CLIP tetramers (data not shown).

α3(IV)NC1 peptides and proteins. The human $\alpha3_{135-145}$ peptide (GWISLWKGFSF), the mouse $\alpha3_{136-146}$ peptide (DWVSLWKGFSF) and control $OVA_{323-339}$ peptide (ISQAVHAAHAEINEAGR) was synthesized at >95% purity, confirmed by HPLC (Mimotopes). Recombinant murine α3(IV)NC1 was generated using a baculovirus system[21] and recombinant human α3(IV)NC1 expressed in HEK 293 cells[22]. The murine α3(IV)NC1 peptide library, which consists of 28 20 amino acid long peptides overlapping by 12 amino acids, was synthesized as a PepSet (Mimotopes).

Reactivity to α3(IV)NC1 T cell epitopes. To measure peptide specific recall responses, IFN-γ and IL-17A ELISPOTs and [^{3}H]-T proliferation assays were used (Mabtech for human ELISPOTs and BD Biosciences for mouse ELISPOTs). To measure pro-inflammatory responses of HLA-DR15-$\alpha3_{135-145}$ $tetramer^+$ $CD4^+$ T cells in patients with Goodpasture's disease, HLA-DR15-$\alpha3_{135-145}$ $tetramer^+$ $CD4^+$ T cells were enumerated then isolated from peripheral blood mononuclear cells of patients with Goodpasture's disease (frozen at time of presentation) by magnetic bead separation (Miltenyi Biotec) then co-cultured at a frequency of 400 HLA-DR15-$\alpha3_{135-145}$ $tetramer^+$ $CD4^+$ T cells/well with 2 x 10^6 HLA-DR15-$\alpha3_{135-145}$ tetramer depleted mitomycin C treated white blood cells and stimulated with either no antigens, $\alpha3_{135-145}$ (10μg/ml) or whole recombinant human α3(IV)NC1 (10μg/ml) in supplemented RPMI media (10% male AB serum, 2mM L-Glutamine, 50 μM 2-ME, 100 U/ml penicillin and 0.1 mg/ml streptomycin) (Sigma-Aldrich). Cells were cultured for 18 hours at 37˚C, 5% CO_2 and the data expressed as numbers of IFN-γ or IL-17A spots per well. To measure pro-inflammatory responses of HLA-DR15-$\alpha3_{135-145}$ $tetramer^+$ $CD4^+$ T cells in $DR15^+$ transgenic mice, HLA-DR15-$\alpha3_{135-145}$ $tetramer^+$ $CD4^+$ T cells were enumerated then isolated from pooled spleen and lymph node cells of $DR15^+$ transgenic mice, immunized with mouse $\alpha3_{136-146}$ 10 days prior, by magnetic bead separation then co-cultured at a frequency of 400 HLA-DR15-$\alpha3_{135-145}$ $tetramer^+$ $CD4^+$ T cells/well with 10^6 HLA-DR15-$\alpha3_{135-145}$ tetramer depleted mitomycin C treated white blood cells and stimulated with either no antigens, mouse $\alpha3_{136-146}$ (10μg/ml), human $\alpha3_{135-145}$ (10μg/ml), whole recombinant mα3(IV)NC1 (10μg/ml) or whole recombinant hα3(IV)NC1 (10μg/ml) in supplemented RPMI media (10% FCS,

2mM L-Glutamine, 50 μM 2-ME, 100 U/ml penicillin and 0.1 mg/ml streptomycin). Cells were cultured for 18 hours at 37˚C, 5% CO_2 and the data expressed as numbers of IFN-γ or IL-17A spots per well. To determine the immunogenic portions of α3(IV)NC1, mice were immunized subcutaneously with either peptide pools (containing α3 aa 1-92, 81-64, or 153-233; 10 μg/peptide per mouse), the individual peptide or in some experiments m$\alpha3_{136\text{-}146}$ at 10 μg/mouse in Freund's complete adjuvant (Sigma-Aldrich). Draining lymph node cells were harvested 10 days after immunization and stimulated *in vitro* (5 x 10^5 cells/well) with no antigen, peptide (10 μg/ml) or whole α3(IV)NC1 (10 μg/ml) in supplemented RPMI media (10% FCS, 2mM L-Glutamine, 50 μM 2-ME, 100 U/ml penicillin and 0.1 mg/ml streptomycin). For [^{3}H]-T proliferation assays, cells were cultured in triplicate for 72 hours with [^{3}H]-T added to culture for the last 16 h. To measure human $\alpha3_{135\text{-}145}$ or mouse $\alpha3_{136\text{-}146}$-specific responses in $CD4^+$ T cells from naïve transgenic mice or blood of healthy humans, we used a modification of a previously published protocol[23], 10^6 $CD4^+$ T cells were cultured with 10^6 mitomycin-treated CD4-depleted splenocytes for 8 days in 96-well plates with or without 100 μg/ml of human $\alpha3_{135\text{-}145}$ or mouse $\alpha3_{136\text{-}146}$. Tregs were depleted from mouse cultures by sorting out $CD4^+CD25^+$ and in humans by sorting out $CD4^+CD25^{hi}CD127^{lo}$ cells using antibodies and a cell sorter. Cytokine secretion was detected in the cultured supernatants by cytometric bead array (BD Biosciences) or ELISA (R&D Systems). To determine proliferation, magnetically separated $CD4^+$ T cells were labeled with CTV (Thermo Scientific) prior to culture. To measure the expansion of Tfh cells, mice were immunized with 100 μg of $\alpha3_{135\text{-}145}$ emulsified in FCA, then boosted 7 days later in FIA. Draining lymph node cells were stained with the HLA-DR15-$\alpha3_{135\text{-}145}$ tetramer, CD3, CD4, CXCR5, PD-1, CD8 and Live/Dead Viability dye. To determine the potency of HLA-DR1-$\alpha3_{135\text{-}145}$ tetramer$^+$ Tregs, 10^6 cells/well of $CD4^+CD25^-$ T effectors (Teff) isolated by $CD4^+$ magnetic bead and $CD25^-$ cell sorting from naïve $DR15^+DR1^+$ mice was co-cultured with either $CD4^+CD25^+$ Tregs with or without depletion of HLA-DR1-$\alpha3_{135\text{-}145}$ tetramer$^+$ Tregs from $DR1^+$ mice at different concentrations: 0, 12.5 x 10^3, 25 x 10^3, 50 x 10^3, and 100 x 10^3 cells/well in the presence of 10^6 CD4-depleted mitomycin C treated spleen and lymph node cells from $DR15^+DR1^+$mice in supplemented RPMI media (10% FCS, 2mM L-Glutamine, 50 μM 2-ME, 100 U/ml penicillin and 0.1 mg/ml streptomycin) containing 100μg/ml of mouse $\alpha3_{135\text{-}145}$. To determine proliferation, the $CD4^+CD25^-$ Teff cells were labeled with CTV prior to culture. Cells were cultured in triplicate for 8 days in 96-well plates.

Induction and assessment of experimental autoimmune anti-GBM[4]. HLA transgenic mice, on an *Fcgr2b*$^{-/-}$ background, were immunized with 100 μg of $\alpha3_{135\text{-}145}$ or $m\alpha3_{136\text{-}146}$ subcutaneously on days 0, 7, and 14; first in Freund's complete, and then in Freund's incomplete adjuvant. Mice were killed on day 42. Albuminuria was assessed on urine collected during the last 24 h by ELISA (Bethyl Laboratories) and expressed as mg per μmol urine creatinine. BUN and urine creatinine were measured using an autoanalyser at Monash Health. Glomerular necrosis and crescent formation were assessed on PAS-stained sections; fibrin deposition using anti-murine fibrinogen antibody (R-4025) and DAB (Sigma); $CD4^+$ T cells, macrophages and neutrophils were detected using anti-CD4 (GK1.5), anti-CD68 (FA/11) and anti-Gr-1 (RB6-8C5) antibodies. To deplete regulatory T cells, mice were injected intraperitoneally with 1 mg of anti-CD25 mAb (clone PC61) or rat IgG (control) 2 days before induction of disease.

Single-cell multiplexed RT-PCR. Individual DR15-$\alpha3_{135\text{-}145}$-specific $CD4^+$ T cells were sorted into wells of a 96-well plate. Multiplex single-cell reverse transcription and PCR amplification of TCR CDR3α and CDR3β regions was performed using a panel of TRBV- and TRAV-specific oligonucleotides, as described[24,25]. Briefly, mRNA was reverse transcribed in 2.5μl using the Superscript III VILO cDNA Synthesis Kit (Thermo Fisher Scientific, Waltham, MA, USA) (containing 1x Vilo reaction mix, 1x superscript RT, 0.1% Triton X-100), and incubated at 25°C for 10 min, 42°C for 120 min and 85°C for 5 min. The entire volume was then used in a 25μl first-round PCR reaction with 1.5U *Taq* DNA polymerase, 1x PCR buffer, 1.5mM $MgCl_2$, 0.25mM dNTPs and a mix of 25 mouse TRAV or 40 human TRAV external sense primers and a TRAC external antisense primer, along with 19 mouse TRBV or 28 human TRBV external sense primers and a TRBC external antisense primer (each at 5 pmol μl^{-1}), using standard PCR conditions. For the second-round nested PCR, a 2.5 μl aliquot of the first-round PCR product was used in separate TRBV- and TRAV-specific PCRs, using the same reaction mix described above; however, a set of 25 mouse TRAV or 40 human TRAV internal sense primers and a TRAC internal antisense primer, or a set of 19 mouse TRBV or 28 human TRBV internal sense primers and a TRBV internal antisense primer, were used. Second-round PCR products were visualized on a gel and positive reactions were purified with ExoSAP-IT reagent. Purified products were used as template in sequencing reactions with internal TRAC or TRBC antisense primers, as described. TCR gene segments were assigned using the IMGT (International

ImMunoGeneTics) database[26]. In mouse experiments, 3 mice were pooled per HLA and the number of sequences obtained were for TRAV (DR15, *n* = 81; DR1 *n* = 84), for TRBV (DR15, *n* = 100; DR1 *n* = 87), for TRAJ (DR15, *n* = 81; DR1 *n*= 84) and for TRBJ (DR15, *n* = 100; DR1 *n* = 87).

RT-PCR for tTreg genes. Red blood cell lysed splenocytes from $DR1^+$ and $DRB15^+DR1^+$ mice were sorted based on surface expression of CD4 and CD25 and either DR1-$\alpha3_{135\text{-}145}$ tetramer positive or negative into three groups, 1) $CD4^+CD25^-$HLA-DR1-$\alpha3_{135\text{-}145}$ $tetramer^-$ T conventional (Tconv) cells, 2) $CD4^+CD25^+$HLA-DR1-$\alpha3_{135\text{-}145}$ $tetramer^-$ Tregs, and 3) $CD4^+CD25^+$HLA-DR1-$\alpha3_{135\text{-}145}$ $tetramer^+$ Tregs. A minimum of 1000 cells were sorted. Immediately after sorting the RNA was isolated and cDNA generated using the Cells to Ct Kit (Ambion) followed by a preamplification reaction using Taqman Pre Amp Master Mix (Applied Biosystems) which preamplified the following cDNAs: *Il2ra*, *Foxp3*, *Ctla4*, *Tnfrsf18*, *Il7r*, *Sell*, *Pdcd1*, *Entpd1*, *Cd44*, *Tgfb3*, *Itgae*, *Ccr6*, *Lag3*, *Lgals1*, *Ikzf2*, *Tnfrsf25*, *Nrp1*, *Il10*. The preamplified cDNA was used for RT-PCR reactions in duplicate using Taqman probes for the aforementioned genes. Each gene is expressed relative to *18s*, logarithmically transformed and presented as a heat map.

Purification of MHC bound peptides. The EBV transformed human B lymphoblastoid cell lines IHW09013 (SCHU, DR15-DR51-DQ6) and IHW09004 (JESTHOM, DR1-DQ5) were maintained in RPMI (Invitrogen) supplemented with 10% FCS, 50 IU/ml penicillin and 50 μg/ml streptomycin. Confirmatory tissue typing of these cells was performed by the Victorian Transplantation and Immunogenetics Service. The B cell hybridoma LB3.1 (anti-DR) was grown in RPMI-1640 with 5% FCS at 37°C and secreted antibody purified using protein A sepharose (BioRad). HLA-DR presented peptides were isolated from naïve $DR15^{+.Fcgr2b+/+}$ or $DR1^{+.Fcgr2b+/+}$ mice. Spleens and lymph nodes (pooled from five mice in each group) or frozen pellets of human BLCLs (triplicate samples of 10^9 cells) were cryogenically milled and solubilised as previously described[12,27], cleared by ultracentrifugation and MHC peptide complexes purified using LB3.1 coupled to protein A (GE Healthcare). Bound HLA complexes were eluted from each column by acidification with 10% acetic acid. The eluted mixture of peptides and HLA heavy chains was fractionated by RP-HPLC as previously described[10].

LC-MS/MS acquisition and analysis. Peptide-containing fractions were analysed by nano-LC-MS/MS using a ThermoFisher Q-Exactive Plus mass spectrometer (ThermoFisher Scientific, Bremen, Germany) operated as described previously[10]. LC-MS/MS data was searched against the mouse or human proteomes (Uniprot/Swissprot v2016_11) using the ProteinPilot™ software (SCIEX) and resulting peptide identities subject to strict bioinformatic criteria including the use of a decoy database to calculate the false discovery rate (FDR)[28]. A 5% FDR cut-off was applied, and the filtered dataset was further analysed manually to exclude redundant peptides and known contaminants as previously described[29]. The mass spectrometry data have been deposited to the ProteomeXchange Consortium via the PRIDE[30] partner repository with the dataset identifier PXD005935.

Motif Analysis. Minimal core sequences found within nested sets of peptides with either N- or C-terminal extensions were extracted and aligned using MEME (http://meme.nbcr.net/meme/), where motif width was set to 9-15 and motif distribution set to 'one per sequence'[31]. Graphical representation of the motif was generated using IceLogo[32].

Crystallization and structure determination. Crystal trials were set-up at 21°C using the hanging drop vapour diffusion method. Crystals of HLA-DR15-$\alpha 3_{135\text{-}145}$ were grown in 25% PEG 3350, 0.2M KNO_3 and 0.1M Bis-Tris-propane (pH 7.5), and crystals of HLA-DR1-$\alpha 3_{135\text{-}145}$ were grown in 23% PEG 3350, 0.1M KNO_3, and 0.1M bis-tris-propane (pH 7.0). Crystals were washed with mother liquor supplemented with 20 % ethylene glycol and flash frozen in liquid nitrogen prior to data collection. Data was collected using the MX1 beamline[33] at the Australian Synchrotron, and processed with iMosflm and Scala from the CCP4 program suite[34]. The structures were solved by molecular replacement in PHASER[35] and refined by iterative rounds of model building using COOT[36] and restrained refinement using Phenix[37] (see **Extended Data Table 2** for data collection and refinement statistics).

Statistics. For normally distributed data, an unpaired two-tailed *t*-test (when comparing two groups) or one-way ANOVA (Tukey post-test) was used. For non-normally distributed data, non-parametric tests (Mann-Whitney for two groups or Kruskal-Wallis test with Dunn's multiple comparison) were used. Statistical analyses, except for TCR usage, was by GraphPad Prism (GraphPad Software Inc.). For each TCR type/region (TRAV, TRBV, TRAJ, TRBJ), we compared the TCR distribution (frequencies of different TCRs) between

DR15 and DR1 using Fisher's exact test. This was applied to both mice and human samples. The p-values associated with those TCR distributions are indicated above the pie-charts. To correct for multiple testing for individual TCR, we used Holm's method. *P<0.05, **P<0.01, ***P<0.001.

Data Availability Statement

The data that support the findings of this study are available from the corresponding authors upon request. Self-peptide repertoires have been deposited in the PRIDE archive with the accession code PXD005935. Structural information has been deposited in PDB under accession codes 5V4M and 5V4N.

EXTENDED DATA TABLES

Extended Data Table 1. Clinical details of patients with anti-GBM glomerulonephritis

Patient	Gender	Age	Serum creatinine (μmol/L)	Treatment at sampling
GP1	Male	72	1300	CS, CYC
GP2	Female	19	184	Nil
GP3	Male	55	1991 *	CS, PLEX
GP4	Female	72	369	CS, PLEX, CYC
GP5	Female	86	600 *	Nil
GP6	Male	72	730	CS, PLEX, CYC
GP7	Female	25	212	CS, PLEX, CYC
GP8	Female	79	492	Nil

***** Receiving hemodialysis at the time of sampling

CS, corticosteroids; PLEX, plasma exchange, CYC, cyclophosphamide

Extended Data Table 2: Data collection and refinement statistics

	HLA-DR15-$\alpha3_{135\text{-}145}$ (5V4M)	HLA-DR1-$\alpha3_{135\text{-}145}$ (5V4N)
Data collection		
Space group	P1	$P2_12_12_1$
Cell dimensions		
a, *b*, *c* (Å)	67.59, 79.01, 95.82	82.09, 118.41, 120.88
α, β, γ (°)	87.64, 73.29, 89.97	90, 90, 90
Resolution (Å)	48.32-2.1 (2.18-2.1)[a]	53.831-3.405 (3.527-3.405) [a]
R_{merge}	0.129 (0.709)	0.1099 (0.3648)
$I/\sigma(I)$	9.5 (2.3)	6.04 (2.60)
$CC_{1/2}$	0.995(0.692)	0.942 (0.651)
Completeness (%)	96.3 (95.5)	99.0 (99.0)
Redundancy	5.4 (5.3)	2.0 (2.0)
Refinement		
Resolution (Å)	48.32-2.1	53.831-3.405
No. reflections	106601	16628
R_{work} / R_{free}	0.2167/0.2440	0.2121/0.2629
No. atoms	13352	6194
Protein	12518	6152
Ligand/ion	180	42
Water	654	-
B factors		
Protein	34.96	67.59
Ligand/ion	71.88	113.48
Water	37.15	-
R.m.s. deviations		
Bond lengths (Å)	0.003	0.003
Bond angles (°)	0.67	0.72

Number of crystals for each structure should be noted in footnote.
[a] Values in parentheses are for highest-resolution shell.

Extended Data Table 3. HLA type of healthy human donors (HD, healthy donor)

DR15 homozygotes

Donor	A	B	C	Bw	DRB1	DQBI	DPB1	DRB5
HD1	1, 24	24, 8	7		15:01	6	4, 16	1:01
HD2	2, 3	7, 15	3, 7	6	15:01	6	4	1:01
HD3	2, 3	7, 51	7, 14	4, 6	15:01	6		
HD4	3, 11	7, 47	6, 7	4, 6	15:01	6		
HD5	1, 29	7	7	6	15:01			
HD6	1, 2	7	7	6	15:01	6		1:01

DR1 homozygotes

	A	B	C	Bw	DRB1	DQBI	DPB1	DRB5
HD7	3, 11	35, 62	3, 4		01:01	5		
HD8	3, 24	51, 40	3, 14	4, 6	01:01			
HD9	2, 3	51, 56	1	4, 6	01:01	5		
HD10	2, 3	27, 35		4, 6	01:01	5		
HD11	3, 26	27, 35	1, 4	4, 6	01:01	5	4	

DR15/DR1 heterozygotes

	A	B	C	Bw	DRB1	DQBI	DPB1	DRB5
HD12	3, 29	7, 35	04, 07	6	01:01, 15:01	5, 6	4	1:01
HD13	3, 26	7, 27	1, 7	4, 6	01:01, 15:01	5, 6	4	1:01
HD14	03, 26	7, 49	7	4, 6	01:01, 15:01	5, 6	3, 4	1:01
HD15	03	7, 14	7, 8		01:01, 15:01	5, 6		
HD16	02, 03	7, 51		4, 6	01:01, 15:01	5, 6		1:01

EXTENDED DATA FIGURE LEGENDS

Extended Data Figure 1: HLA-DR15-α3$_{135\text{-}145}$ tetramer^{+} CD4^{+} T cells from humans and mice respond to α3$_{135\text{-}145}$ and to whole α3(IV)NC1. a, HLA-DR15-α3$_{135\text{-}145}$ tetramer^{+} CD4^{+} T cells isolated from patients with Goodpasture's disease (*n*=8) respond to α3$_{135\text{-}145}$ and recombinant human (rh)α3(IV)NC1. HLA-DR15-α3$_{135\text{-}145}$ tetramer^{+} CD4^{+} T cells were isolated by magnetic bead separation from the blood of patients with Goodpasture's disease, then cultured at a frequency of 400 HLA-DR15-α3$_{135\text{-}145}$ tetramer^{+} CD4^{+} T cells per well in the presence of mitomycin C treated HLA-DR15-α3$_{135\text{-}145}$ tetramer^{+} cell depleted white blood cells and either hα3$_{135\text{-}145}$ or rhα3(IV)NC1. Antigen specific responses were assessed by ELISPOTs for IFN-γ and IL-17A and expressed as numbers of spots per well. **b**, To induce experimental autoimmune anti-GBM disease, DR15$^{+.Fcgr2b\text{-}/\text{-}}$ mice (*n*=5) were immunized with hα3$_{135\text{-}145}$ on days 0, 7 and 14. Disease was measured at day 42, by which time DR15$^{+.Fcgr2b\text{-}/\text{-}}$ mice develop kidney disease similar to human Goodpasture's disease including glomerular segmental necrosis, crescents (PAS stain), linear IgG deposition (direct immunofluorescence) and pathological albuminuria. Each dot represents one mouse. Photomicrographs taken at 400x depict a crescentic glomerulus with segmental necrosis (bottom left panel) and linear glomerular IgG deposition (bottom right panel) seen in DR15$^{+.Fcgr2b\text{-}/\text{-}}$ mice immunized with hα3$_{135\text{-}145}$. Scale bars = 30μm. **c**, HLA-DR15-α3$_{135\text{-}145}$ tetramer^{+} CD4^{+} T cells isolated from DR15$^{+.Fcgr2b+/+}$ mice respond to mouse (m)α3$_{136\text{-}146}$, hα3$_{135\text{-}145}$, rmα3(IV)NC1 and rhα3(IV)NC1. HLA-DR15-α3$_{135\text{-}145}$ tetramer^{+} CD4^{+} T cells were isolated by magnetic bead separation from pooled spleen and lymph node cells of two DR15^{+} transgenic mice 10 days after immunisation with mα3$_{136\text{-}146}$ (DWVSLWKGFSF, hα3$_{135\text{-}145}$ GWISLWKGFSF) then cultured at a frequency of 400 HLA-DR15-α3$_{135\text{-}145}$ tetramer^{+} CD4^{+} T cells per well in the presence of mitomycin C treated HLA-DR15-α3$_{135\text{-}145}$ tetramer^{+} cell depleted spleen and lymph node cells. Antigen specific responses were assessed by ELISPOTs for IFN-γ and IL-17A and expressed as numbers of spots per well. $^{*}P$<0.05; $^{**}P$<0.01; $^{***}P$<0.001 by Kruskal-Wallis test (**a** and **c**) or Mann-Whitney U test (**b**).

Extended Data Figure 2: Immune responses in DR15^{+}DR1$^{+.Fcgr2b+/+}$ mice. a, Naïve FcγRIIb intact HLA transgenic mice have similar immune properties. Shown are the proportion of splenocytes expressing HLA-DR; HLA-DR15 and HLA-DR1 intensities (MFI) in naïve DR15^{+} (*n*=4), DR1^{+} (*n*=4) and DR15^{+}DR1^{+} transgenic mice (*n*=5) showing half the amount of expression in DR15^{+}DR1^{+} relative to its single transgenic counterpart; total number of splenocytes; proportion of CD4^{+} and CD4^{+}Foxp3^{+} splenocytes; total number of lymph node cells retrieved from the brachial, axillary and inguinal lymph nodes; proportion of CD4^{+} and CD4^{+}Foxp3^{+} lymph node cells and the overall Vβ repertoire of HLA transgenic mice showing no skewing of any one Vβ chain. Data expressed as mean±s.e.m., analysed by ANOVA. **b**, Co-expression of HLA-DR1 abrogates pro-inflammatory high autoreactivity to peptide mα3$_{129\text{-}148}$ but not to other parts of α3(IV)NC1. FcγRIIb intact DR15^{+}, DR1^{+} and DR15^{+}DR1^{+} mice were immunized with murine α3 peptide pools (see Methods for peptide pools) (*n* = 5 each group) and responses to individual 20-mer peptides measured by restimulating the draining lymph node cells *ex vivo* (*x*-axis numbering represents the N-terminus amino acid number of the individual 20-mer peptide) using [^{3}H]-T proliferation assays, and IFN-γ and IL-17A ELISPOTs. Each dot represents the mean response from triplicate determinations in an individual mouse and each bar represents the mean response in each group. Blue bars indicate no reactivity (SI < 2; spots < 5), yellow bars indicate low reactivity (2 < SI < 5; 5 < spots < 25), and red bars indicate high reactivity (SI > 5, spots > 25).

Extended Data Figure 3: Self-peptide repertoires of HLA-DR15/DR51 and HLA-DR1 using human cell lines, with electron density maps for the $\alpha 3_{135\text{-}145}$ peptide. Peptide repertoire analysis of 9-mer core sequences of HLA-DR presented self-peptides in the human BLCLs IHW09013 ($DR15^+/DR51^+$) and IHW09004 ($HLA\text{-}DR1^+$). Amino acid frequencies in each peptide position p1 to p9 were plotted using IceLogo[32], with the human proteome as the frequency reference. Relatively enriched amino acids are plotted above the horizontal bar, and depleted amino acids below. The scale of each letter is proportional to the frequency difference to the reference. Peptides were eluted from **a**, IHW09013 $HLA\text{-}DR15^+/DR51^+$ cells, and **b,** from IHW09004 $HLA\text{-}DR1^+$ cells. For HLA-DR1, preferred amino acids at p1, p4, p6, p7 and p9 are similar between the human and mouse $DR1^+$ cells. For $DR15^+/DR51^+$ human cells compared to $DR15^+$ mouse APCs, the difference at p9, with Lys and Arg being the most frequently bound residues, reflects the known DR51-related motif. **c**, **d**, Simulated annealing $2F_{obs}\text{-}F_{calc}$ omit maps for the peptide of **c**, HLA-DR15 and **d**, HLA-DR1. **e**, **f**, Final $2F_{obs}\text{-}F_{calc}$ maps for the peptide in **e**, HLA-DR15 and **f**, HLA-DR1. Electron density maps contoured at 1σ are shown as blue mesh.

Extended Data Figure 4: HLA-DR1-α3$_{135-145}$ tetramer^{+} CD4^{+} T cells have differential TRAJ usage and the CD4^{+}CD25^{+} Tregs gene transcription profile is similar to that of thymically derived Tregs (tTregs). a, The TRAJ and TRBJ usage of α3$_{135-145}$-specific CD4^{+} T cells was compared using the HLA-DR15-α3$_{135-145}$ tetramer (in naïve DR15^{+} *Fcgr2b*$^{+/+}$ mice) and the HLA-DR1-α3$_{135-145}$ tetramer (in naïve DR1^{+}.*Fcgr2b*$^{+/+}$ mice) by single cell sequencing. α3$_{135-145}$-specific CD4^{+} tetramer^{+} T cells from naïve DR15^{+} (*n*=3) and DR1^{+} (*n*=3) transgenic mice were pooled then single cell sorted, TCR genes amplified by multiplex PCR, then sequenced to determine TRAJ (DR15, *n*=81; DR1 *n*=84) and TRBJ (DR15, *n*=100; DR1 *n*=87) usage. For each TCR type/region (TRAV, TRBV, TRAJ, TRBJ; TRAV and TRBV shown in **Fig. 2g**), we compared the TCR distribution (frequencies of different TCRs) between DR15 and DR1, *** P<0.001 by Fisher's exact test. **b**, HLA-DR1-α3$_{135-145}$ tetramer^{-} CD4^{+}CD25^{-} Tconv, HLA-DR1-α3$_{135-145}$ tetramer^{-}CD4^{+}CD25^{+} Tregs and HLA-DR1-α3$_{135-145}$ tetramer^{+} CD4^{+}CD25^{+} Tregs were isolated from naïve FcγRIIb intact DR1^{+} or DR15^{+}DR1^{+} transgenic mice by flow cytometry, RNA extracted and the relative expression of tTreg genes expressed relative to *18S*. The HLA-DR1-α3$_{135-145}$ tetramer^{+} CD4^{+}CD25^{+} Tregs express genes consistent with a tTreg origin, similar to other Tregs that are not α3$_{135-145}$-specific from the same mice.

Extended Data Figure 5: Responses and effects of antigen specific DR1-associated Tregs. a, Measurement of pro- and anti-inflammatory mouse (m)$\alpha3_{136\text{-}146}$-specific $CD4^+$ T cell responses by *ex vivo* stimulation. $CD4^+$ T cells, isolated and pooled from naïve $DR15^{+.Fcgr2b+/+}$ (*n*=2), $DR1^{+.Fcgr2b+/+}$ (*n*=2) and $DR15^+DR1^{+.Fcgr2b+/+}$ (*n*=2) transgenic mice were cultured for 8 days in the presence of m$\alpha3_{136\text{-}146}$ and mitomycin C treated syngeneic $CD4^+$ cell-depleted splenocytes. Tregs were depleted by removing $CD4^+CD25^+$ T cells by cell sorting. IFN-γ, IL-17A, IL-6 and IL-10 were measured in the cultured supernatant by cytometric bead array and TGF-β by ELISA. The experiment was performed in triplicate and the data presented as mean±s.e.m. To measure $\alpha3_{136\text{-}146}$-specific $CD4^+$ Treg proliferation, $CD4^+$ T cells were labelled with CTV then stained with Foxp3 on day 8. Results were similar to those performed using human (h)$\alpha3_{135\text{-}145}$ presented in **Fig. 3b**. **b**, HLA-DR1-$\alpha3_{135\text{-}145}$-specific Tregs are potent suppressors of HLA-DR15-$\alpha3_{135\text{-}145}$ induced pro-inflammatory responses. $CD4^+CD25^-$ T cells were isolated and pooled from naïve $DR15^+DR1^{+.Fcgr2b+/+}$ mice (*n*=2) and co-cultured with either $CD4^+CD25^+$ Tregs (which included HLA-DR1-$\alpha3_{135\text{-}145}$ $tetramer^+$ Tregs) or $CD4^+CD25^+$ HLA-DR1-$\alpha3_{135\text{-}145}$ $tetramer^-$ from naïve $DR1^{+.Fcgr2b+/+}$ mice (*n*=4) in the presence of m$\alpha3_{136\text{-}146}$ and $CD4^+$ cell-depleted spleen and lymph node cells from $DR15^+DR1^+$ mice. Cells were cultured for 8 days. $\alpha3_{135\text{-}145}$-specific $CD4^+CD25^-$ cell proliferation was measured by labelling only the $DR15^+DR1^+$ derived naïve $CD4^+CD25^-$ cells with CTV; IFN-γ, IL-17A, IL-6 and IL-10 were measured in the cultured supernatant by cytometric bead array. In the absence of $CD4^+CD25^+$ HLA-DR1-$\alpha3_{135\text{-}145}$ $tetramer^+$ cells, the capacity of Tregs to prevent the induction of autoreactivity to $\alpha3_{135\text{-}145}$ was impaired. These experiments were performed in triplicate and the data presented as mean±s.e.m. **c**, Treg depletion expands HLA-DR15-$\alpha3_{135\text{-}145}$-specific T follicular helper (Tfh) cells. Anti-CD25 mAbs (or control Rat IgG) were administered 2 days prior to h$\alpha3_{135\text{-}145}$ immunization and boost (*n*=4 per group), then the number of $\alpha3_{135\text{-}145}$-specific PD-1^+CXCR5^+ Tfh cells enumerated in the draining lymph nodes. FACS plots show the expansion of $PD1^+CXCR5^+$ Tfh cells after Treg depletion and the detection of HLA-DR15-$\alpha3_{135\text{-}145}$-specific cells within that population. $^*P < 0.05$; $^{**}P < 0.01$; $^{***}P < 0.001$ by Mann-Whitney U test (**a** and **b**) or Kruskal-Wallis test (**c**).

Extended Data Figure 6: *In vivo* Treg depletion in HLA transgenic mice. a, Efficiency and duration of Treg depletion using anti-CD25 mAb (clone PC61) in $DR15^{+}DR1^{+.Fcgr2b-/-}$ mice. Timeline showing the administration of anti-CD25 mAb 2 days before immunizing mice with human (h)$\alpha3_{135-145}$. Detection of $CD4^{+}foxp3^{+}$ Tregs in the blood showing depletion of Tregs at days 7 and 14 in mice that received the anti-CD25 mAb (*n*=5 each group). White bars represent mice that received control antibodies and solid bars represent mice that received anti-CD25 mAb. **b**, $DR15^{+.Fcgr2b-/-}$ (*n*=6 each group), $DR1^{+.Fcgr2b-/-}$ (*n*=4 each group) and $DR15^{+}DR1^{+.Fcgr2b-/-}$ (*n*=6 each group) mice immunized with a control peptide, $OVA_{323-339}$ do not develop renal injury. Functional injury measured by albuminuria and blood urea nitrogen; and histological injury assessed by scoring of PAS stained histological sections for segmental necrosis and glomerular crescents. Representative PAS stained histological sections. White bars represent mice that received control antibodies and solid bars represent mice that received anti-CD25 mAb. **c**, Treg depletion leads to cell mediated injury in $DR15^{+}DR1^{+.Fcgr2b-/-}$ mice (further data collected in the experiment presented in **Fig. 4a**). Anti-CD25 mAbs (or control Rat IgG) were administered 2 days prior to the induction of experimental autoimmune anti-GBM GN by h$\alpha3_{135-145}$ immunization in $DR15^{+.Fcgr2b-/-}$ (*n*=6 per group), $DR1^{+.Fcgr2b-/-}$ (*n*=4 per group) and $DR15^{+}DR1^{+.Fcgr2b-/-}$ (*n*=8 [Treg intact], 9 [Treg depleted]) mice. Cell mediated injury was assessed by quantifying glomerular fibrin deposition and enumerating and inflammatory cell infiltrates ($CD4^{+}$ T cells, macrophages and neutrophils). Renal inflammation was measured by RT-PCR of inflammatory cytokines (TNF, IL-6 and IL-1α) on kidney digests. Scale bars = 30 μm. **d**, Repeating the experiment presented in **Fig. 4a** using mouse (m)$\alpha3_{136-146}$ instead of h$\alpha3_{135-145}$ as the immunogen showed similar results ($DR15^{+.Fcgr2b-/-}$, *n*=6 [Treg intact], 7 [Treg depleted]; $DR1^{+.Fcgr2b-/-}$, *n*=4 [Treg intact], 5 [Treg depleted]; and $DR15^{+}DR1^{+.Fcgr2b-/-}$, *n*=6 per group), with the emergence of autoimmune anti-GBM glomerulonephritis in $DR15^{+}DR1^{+.Fcgr2b-/-}$ mice only after Treg depletion. Values are mean±s.e.m.; $^{*}P < 0.05$; $^{**}P < 0.01$; $^{***}P < 0.001$ by Mann-Whitney U test **(a-d)**.

Extended Data Figure 7: Single cell sequencing data from healthy humans and Goodpasture's patients validate and corroborate findings in HLA transgenic mice. a, Comparing the TCR usage of $\alpha3_{135\text{-}145}$-specific $CD4^+$ T cells using the HLA-DR15-$\alpha3_{135\text{-}145}$ tetramer and the HLA-DR1-$\alpha3_{135\text{-}145}$ tetramer by TCR single cell sequencing, TRAV (DR15, *n*=20; DR1 *n*=28), TRBV (DR15, *n*=20; DR1 *n*=24), TRAJ (DR15, *n*=20; DR1 *n*=28) and TRBJ (DR15, *n*=20; DR1 *n*=24). For each TCR type/region (TRAV, TRBV, TRAJ, TRBJ), we compared the TCR distribution (frequencies of different TCRs) between DR15 and DR1. $^*P < 0.05$ by Fisher's exact test. The full HLA-types of the DR15 homozygous donor (HD1) and the DR1 homozygous donor (HD7) are listed in Extended Data Table 3. **b**, In anti-GBM patients, $\alpha3_{135\text{-}145}$-specific T cells clonally expand. $\alpha3_{135\text{-}145}$-specific $CD4^+$ T cells from the blood of two anti-GBM patients were single cell sorted using HLA-DR15-$\alpha3_{135\text{-}145}$ tetramer by flow cytometry. TCR genes were amplified by multiplex PCR, then sequenced to determine TRAV (*n*=12 and 45) and TRBV usage (*n*=16 and 44) and CDR3 amino acid sequence. Differently coloured slices within the pie chart highlights the TRAV or TRBV in which repeated CDR3 sequences were found. All CDR3 sequences within the highlighted TRAV or TRBV are shown in coloured letters (1 row = 1 CDR3 sequence).

METHODS ASSOCIATED REFERENCES (ONLINE ONLY)

18 Aitman, T. J. *et al.* Copy number polymorphism in Fcgr3 predisposes to glomerulonephritis in rats and humans. *Nature* **439**, 851-855 (2006).

19 Broughton, S. E. *et al.* Biased T cell receptor usage directed against human leukocyte antigen DQ8-restricted gliadin peptides is associated with celiac disease. *Immunity* **37**, 611-621 (2012).

20 Petersen, J. *et al.* T-cell receptor recognition of HLA-DQ2-gliadin complexes associated with celiac disease. *Nat Struct Mol Biol* **21**, 480-488 (2014).

21 Apostolopoulos, J., Ooi, J. D., Odobasic, D., Holdsworth, S. R. & Kitching, A. R. The isolation and purification of biologically active recombinant and native autoantigens for the study of autoimmune disease. *J Immunol Methods* **308**, 167-178 (2006).

22 Netzer, K. O. *et al.* The goodpasture autoantigen. Mapping the major conformational epitope(s) of alpha3(IV) collagen to residues 17-31 and 127-141 of the NC1 domain. *J Biol Chem* **274**, 11267-11274 (1999).

23 Zou, J. *et al.* Healthy individuals have Goodpasture autoantigen-reactive T cells. *J Am Soc Nephrol* **19**, 396-404 (2008).

24 Dash, P. *et al.* Paired analysis of TCRalpha and TCRbeta chains at the single-cell level in mice. *J Clin Invest* **121**, 288-295 (2011).

25 Wang, G. C., Dash, P., McCullers, J. A., Doherty, P. C. & Thomas, P. G. T cell receptor alphabeta diversity inversely correlates with pathogen-specific antibody levels in human cytomegalovirus infection. *Sci Transl Med* **4**, 128ra142 (2012).

26 Lefranc, M. P. *et al.* IMGT, the international ImMunoGeneTics information system. *Nucleic Acids Res* **37**, D1006-1012 (2009).

27 Dudek, N. L. *et al.* Constitutive and inflammatory immunopeptidome of pancreatic beta-cells. *Diabetes* **61**, 3018-3025, doi:10.2337/db11-1333 (2012).

28 Shilov, I. V. *et al.* The Paragon Algorithm, a next generation search engine that uses sequence temperature values and feature probabilities to identify peptides from tandem mass spectra. *Mol Cell Proteomics* **6**, 1638-1655 (2007).

29 Schittenhelm, R. B., Dudek, N. L., Croft, N. P., Ramarathinam, S. H. & Purcell, A. W. A comprehensive analysis of constitutive naturally processed and presented HLA-C*04:01 (Cw4)-specific peptides. *Tissue Antigens* **83**, 174-179 (2014).

30 Vizcaino, J. A. *et al.* 2016 update of the PRIDE database and its related tools. *Nucleic Acids Res* **44**, D447-456 (2016).

31 Bailey, T. L. *et al.* MEME SUITE: tools for motif discovery and searching. *Nucleic Acids Res* **37**, W202-208 (2009).

32 Colaert, N., Helsens, K., Martens, L., Vandekerckhove, J. & Gevaert, K. Improved visualization of protein consensus sequences by iceLogo. *Nat Methods* **6**, 786-787 (2009).

33 Cowieson, N. P. *et al.* MX1: a bending-magnet crystallography beamline serving both chemical and macromolecular crystallography communities at the Australian Synchrotron. *J Synchrotron Radiat* **22**, 187-190 (2015).

34 Winn, M. D. *et al.* Overview of the CCP4 suite and current developments. *Acta Crystallogr D Biol Crystallogr* **67**, 235-242, doi:10.1107/S0907444910045749 (2011).

35 McCoy, A. J. *et al.* Phaser crystallographic software. *J Appl Crystallogr* **40**, 658-674 (2007).

36 Emsley, P., Lohkamp, B., Scott, W. G. & Cowtan, K. Features and development of Coot. *Acta Crystallogr D Biol Crystallogr* **66**, 486-501 (2010).

37 Adams, P. D. *et al.* PHENIX: a comprehensive Python-based system for macromolecular structure solution. *Acta Crystallogr D Biol Crystallogr* **66**, 213-221 (2010).

Figure 1

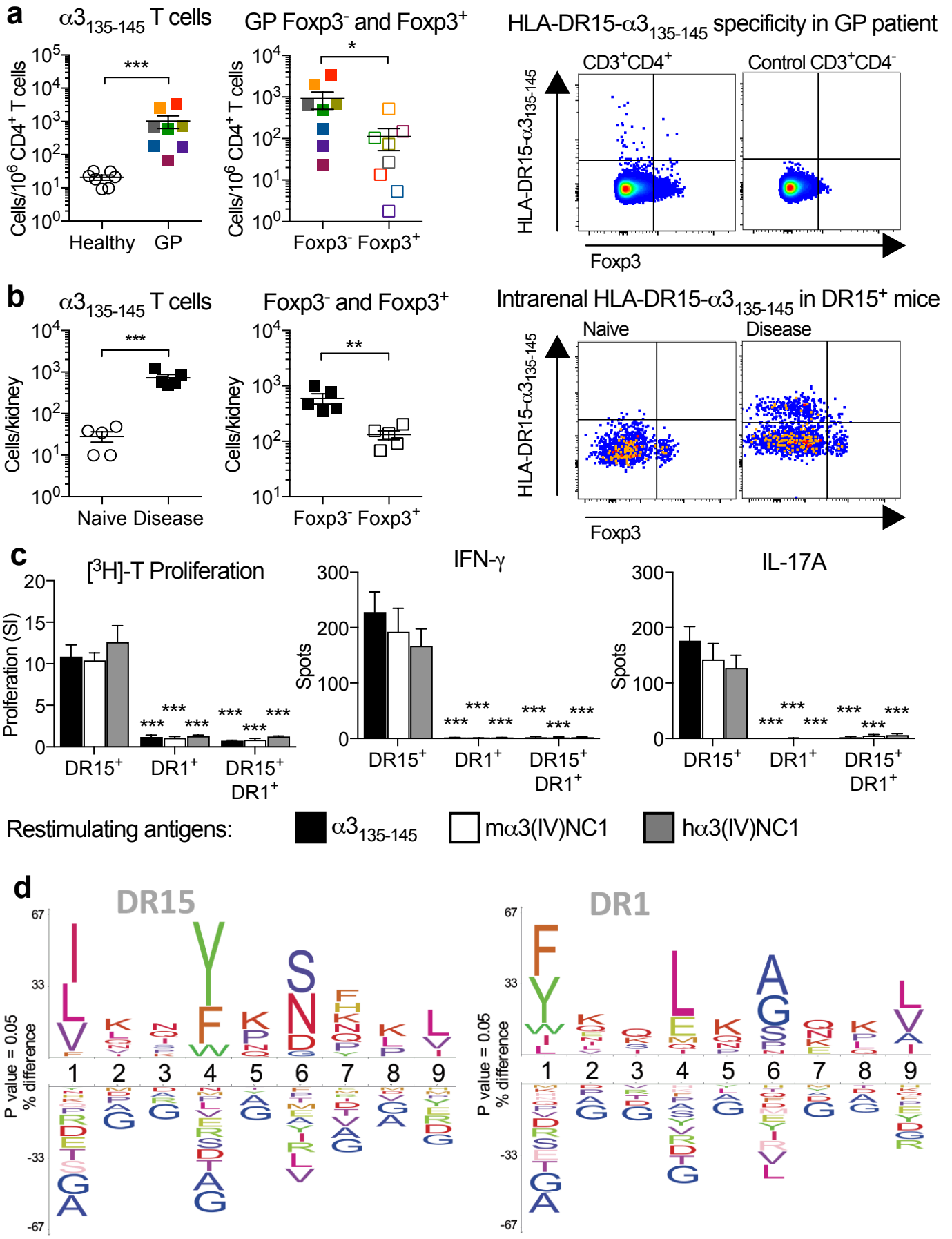
a
α3135-145 T cells
GP Foxp3- and Foxp3+
HLA-DR15-α3135-145 specificity in GP patient
Cells/10^6 CD4+ T cells
Healthy
GP
Foxp3-
Foxp3+
CD3+CD4+
Control CD3+CD4-
HLA-DR15-α3135-145
Foxp3
b
α3135-145 T cells
Foxp3- and Foxp3+
Intrarenal HLA-DR15-α3135-145 in DR15+ mice
Cells/kidney
Naive
Disease
c
[3H]-T Proliferation
IFN-γ
IL-17A
Proliferation (SI)
Spots
DR15+
DR1+
DR15+ DR1+
Restimulating antigens:
α3135-145
mα3(IV)NC1
hα3(IV)NC1
d
DR15
DR1
P value = 0.05
% difference

Figure 2

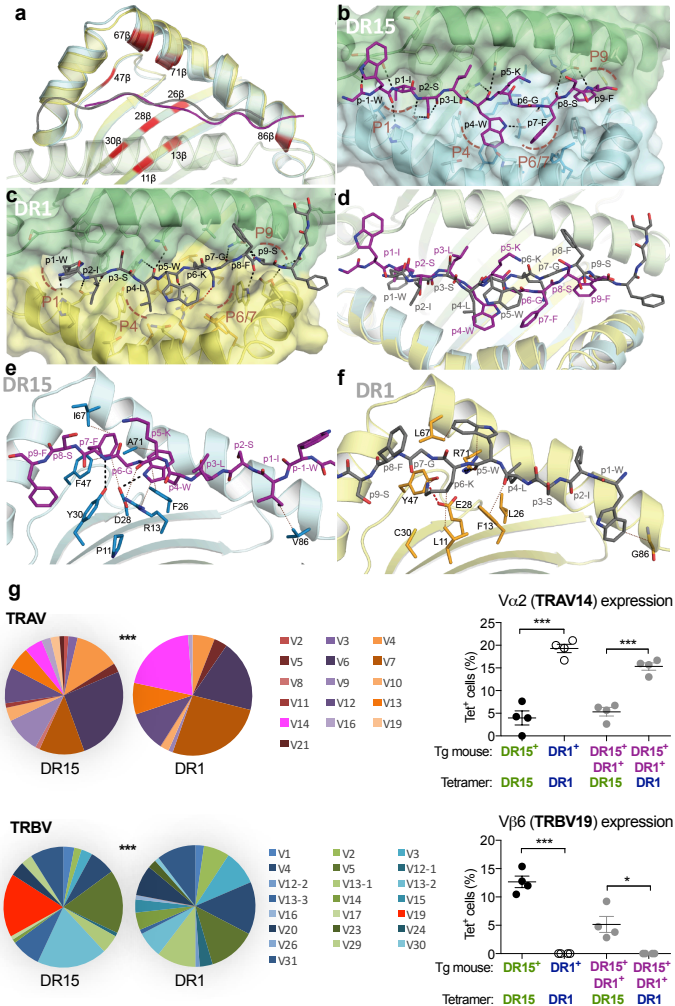
a
67β
71β
47β
26β
28β
30β
86β
13β
11β
b
DR15
P9
p1-I
p2-S
p5-K
p-1-W
p3-L
p6-G
p8-S
p9-F
P1
p4-W
p7-F
P4
P6/7
c
DR1
P9
p1-W
p2-I
p3-S
p5-W
p7-G
p8-F
p9-S
p6-K
P1
p4-L
P4
P6/7
d
p1-I
p3-L
p2-S
p5-K
p6-K
p8-F
p7-G
p9-S
p1-W
p3-S
p8-S
p2-I
p4-L
p6-G
p9-F
p5-W
p7-F
p4-W
e
DR15
I67
A71
p5-K
p7-F
p9-F
p8-S
p2-S
p1-I
p3-L
p1-W
p6-G
F47
p4-W
Y30
F26
D28
R13
P11
V86
f
DR1
L67
R71
p8-F
p7-G
p5-W
p1-W
p6-K
p9-S
p4-L
p2-I
Y47
E28
p3-S
C30
F13
L26
L11
G86
g
TRAV
***
DR15
DR1
V2
V3
V4
V5
V6
V7
V8
V9
V10
V11
V12
V13
V14
V16
V19
V21
Vα2 (TRAV14) expression
***
***
Tet+ cells (%)
25
20
15
10
5
0
Tg mouse:
DR15+
DR1+
DR15+ DR1+
DR15+ DR1+
Tetramer:
DR15
DR1
DR15
DR1
TRBV
***
DR15
DR1
V1
V2
V3
V4
V5
V12-1
V12-2
V13-1
V13-2
V13-3
V14
V15
V16
V17
V19
V20
V23
V24
V26
V29
V30
V31
Vβ6 (TRBV19) expression
***
*
Tet+ cells (%)
20
15
10
5
0
Tg mouse:
DR15+
DR1+
DR15+ DR1+
DR15+ DR1+
Tetramer:
DR15
DR1
DR15
DR1

Figure 3

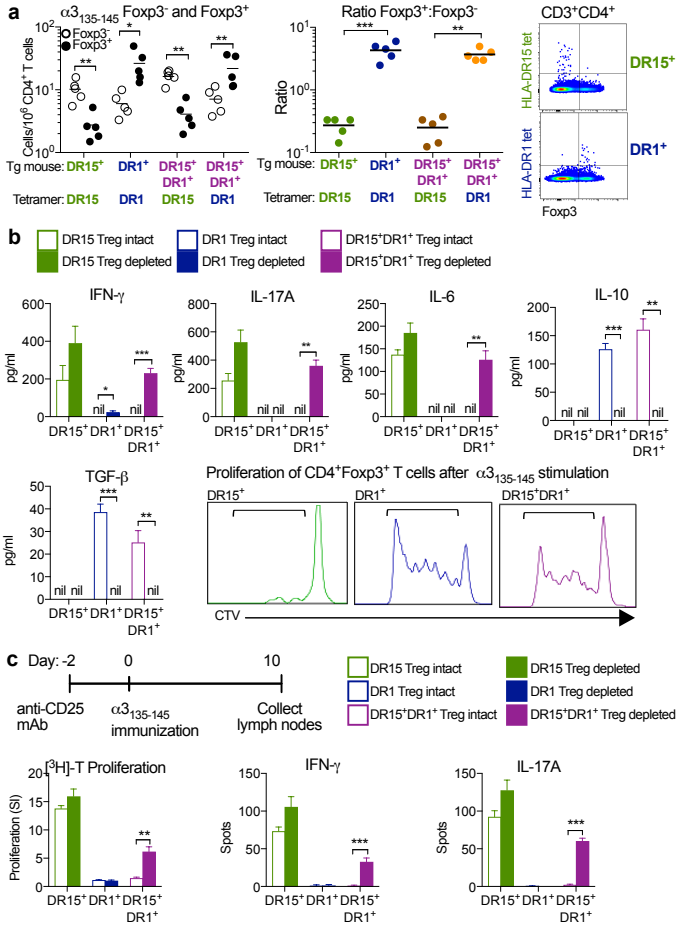
a
α3135-145 Foxp3- and Foxp3+
Foxp3-
Foxp3+
Cells/10^6 CD4+ T cells
Tg mouse: DR15+ DR1+ DR15+ DR1+ DR15+ DR1+
Tetramer: DR15 DR1 DR15 DR1
Ratio Foxp3+:Foxp3-
Ratio
CD3+CD4+
HLA-DR15 tet
HLA-DR1 tet
DR15+
DR1+
Foxp3
b
DR15 Treg intact
DR15 Treg depleted
DR1 Treg intact
DR1 Treg depleted
DR15+DR1+ Treg intact
DR15+DR1+ Treg depleted
IFN-γ
IL-17A
IL-6
IL-10
TGF-β
pg/ml
nil
DR15+ DR1+ DR15+ DR1+
Proliferation of CD4+Foxp3+ T cells after α3135-145 stimulation
DR15+
DR1+
DR15+DR1+
CTV
c
Day: -2
0
10
anti-CD25 mAb
α3135-145 immunization
Collect lymph nodes
DR15 Treg intact
DR15 Treg depleted
DR1 Treg intact
DR1 Treg depleted
DR15+DR1+ Treg intact
DR15+DR1+ Treg depleted
[3H]-T Proliferation
Proliferation (SI)
IFN-γ
IL-17A
Spots

Figure 4

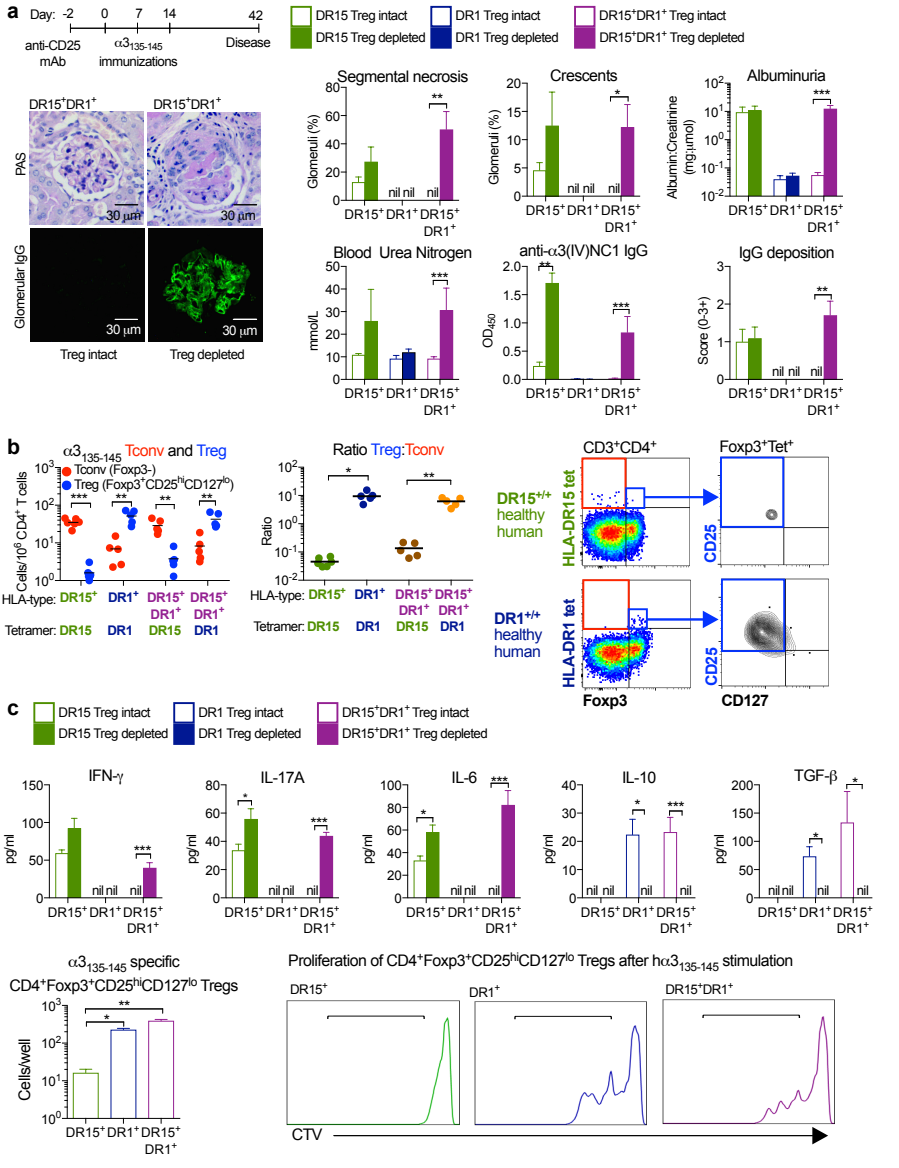
a
Day: -2 0 7 14 42
anti-CD25 mAb
α3135-145 immunizations
Disease
DR15 Treg intact
DR15 Treg depleted
DR1 Treg intact
DR1 Treg depleted
DR15+DR1+ Treg intact
DR15+DR1+ Treg depleted
DR15+DR1+
PAS
Glomerular IgG
30 μm
Treg intact
Treg depleted
Segmental necrosis
Glomeruli (%)
Crescents
Albuminuria
Albumin:Creatinine (mg:μmol)
Blood Urea Nitrogen
mmol/L
anti-α3(IV)NC1 IgG
OD450
IgG deposition
Score (0-3+)
DR15+ DR1+ DR15+ DR1+
b
α3135-145 Tconv and Treg
Tconv (Foxp3-)
Treg (Foxp3+CD25hiCD127lo)
Cells/10^6 CD4+ T cells
HLA-type: DR15+ DR1+ DR15+ DR1+ DR15+ DR1+
Tetramer: DR15 DR1 DR15 DR1
Ratio Treg:Tconv
Ratio
CD3+CD4+
Foxp3+Tet+
DR15+/+ healthy human
DR1+/+ healthy human
HLA-DR15 tet
HLA-DR1 tet
CD25
Foxp3
CD127
c
DR15 Treg intact
DR15 Treg depleted
DR1 Treg intact
DR1 Treg depleted
DR15+DR1+ Treg intact
DR15+DR1+ Treg depleted
IFN-γ
IL-17A
IL-6
IL-10
TGF-β
pg/ml
α3135-145 specific CD4+Foxp3+CD25hiCD127lo Tregs
Cells\well
Proliferation of CD4+Foxp3+CD25hiCD127lo Tregs after hα3135-145 stimulation
DR15+
DR1+
DR15+DR1+
CTV